
THE SUN AND THE HELIOSPHERE
AS AN INTEGRATED SYSTEM

THE SUN AND THE HELIOSPHERE AS AN INTEGRATED SYSTEM

Edited by

GIANNINA POLETTA

INAF, Osservatorio Astrofisico di Arcetri, Firenze, Italy

STEVEN T. SUESS

NSSTC, NASA Marshall Space Flight Center, Huntsville, Alabama, USA

Kluwer Academic Publishers
Boston/Dordrecht/London

A C.I.P. Catalogue record for this book is available from the Library of Congress.

ISBN 1-4020-2830-X (HB)
ISBN 1-4020-2831-8 (e-book)

Published by Kluwer Academic Publishers,
P.O. Box 17, 3300 AA Dordrecht, The Netherlands.

Sold and distributed in North, Central and South America
by Kluwer Academic Publishers,
101 Philip Drive, Norwell, MA 02061, U.S.A.

In all other countries, sold and distributed
by Kluwer Academic Publishers,
P.O. Box 322, 3300 AH Dordrecht, The Netherlands

All Rights Reserved
Copyright 2004 Kluwer Academic Publishers
No part of this work may be reproduced, stored in a retrieval system, or transmitted
in any form or by any means, electronic, mechanical, photocopying, microfilming, recording
or otherwise, without written permission from the Publisher, with the exception
of any material supplied specifically for the purpose of being entered
and executed on a computer system, for exclusive use by the purchaser of the work.

Contents

Preface	xi
1	
Hydrogen Walls: Mass Loss of Dwarf Stars and the Young Sun	1
<i>Jeffrey L. Linsky and Brian E. Wood</i>	
1 Is the Solar Wind Unique?	2
2 Hydrogen Walls: A New Tool for Measuring Mass-Loss Rates	6
2.1 Stellar Astrospheres	12
2.2 The Mass-Loss History of the Sun	17
3 Influence of Stellar Winds on Planets in the Solar System and Beyond	19
4 Conclusions	20
2	
The Heliospheric Interface: Models and Observations	23
<i>Vladislav V. Izmodenov</i>	
1 Introduction	23
2 Brief Summary of Observational Knowledge	26
2.1 Solar Wind Observations	26
2.2 Interstellar Parameters	27
3 Overview of Theoretical Approaches	29
3.1 H Atoms	30
3.2 Solar Wind and Interstellar Electron and Proton Components	32
3.3 Pickup Ions	34
3.4 Cosmic Rays	34
4 Overview of Heliospheric Interface Models	35
5 Self-Consistent Two-Component Model of the Heliospheric Interface and Recent Advancements of the Model	39
5.1 Plasma	39
5.2 H Atoms	42
5.3 Effects of Interstellar and Solar Wind Ionized Helium	45
5.4 Effects of GCRs, ACRs and the Interstellar Magnetic Field	47
5.5 Effects of the Solar Cycle Variations of the Solar Wind	49
5.6 Heliotail	52
6 Interpretations of Spacecraft Experiments Based on the Heliospheric Interface Model	53
6.1 Pickup ions	54
6.2 Location of the Termination Shock in the Direction of Voyager 1	56

	6.3	Filtration of Interstellar Oxygen and Nitrogen	57
7		Summary	57
3			
		Radiation from the Outer Heliosphere and Beyond	65
		<i>Iver H. Cairns</i>	
	1	Introduction	65
	2	Current Observational Status	68
	3	Basic Theoretical Issues	73
	4	The Priming/GMIR Theory	75
	5	Recent Theoretical Results	79
	6	Discussion and Conclusions	85
4			
		Ulysses at Solar Maximum	91
		<i>Richard G. Marsden</i>	
	1	Introduction	91
	2	Scientific Highlights at Solar Maximum	93
		2.1 Solar Wind	94
		2.2 Magnetic Field	99
		2.3 Energetic Particles	101
		2.4 Cosmic Rays	104
		2.5 Interstellar Dust	106
	3	The Future of Ulysses	107
5			
		Propagation of Energetic Particles to High Latitudes	113
		<i>T. R. Sanderson</i>	
	1	Introduction	113
	2	Solar Conditions	115
		2.1 Influence of the Sun on the Heliosphere	115
		2.2 Coronal Magnetic Field During a 22-year Solar Cycle	116
		2.3 Coronal Magnetic Field and Coronal Holes During the Ulysses Mission	119
	3	The First Orbit	120
	4	The Second Orbit	124
		4.1 The Second Polar Passes	125
	5	Discussion	129
		5.1 The Second Northern Polar Pass	129
		5.2 Comparison with the Second Southern Polar Pass	138
	6	Summary and Conclusions	141
6			
		Solar Wind Properties from IPS Observations	147
		<i>Masayoshi Kojima, Ken-ichi Fujiki, Masaya Hirano, Munetoshi Tokumaru, Tomoaki Ohmi and Kazuyuki Hakamada</i>	
	1	Introduction	148
	2	Interplanetary Scintillation Measurements	149
		2.1 Tomographic Analysis of IPS Observations	150
	3	Synoptic Velocity Maps	153
		3.1 Solar Cycle Dependence of Solar Wind Velocity Structure	155
	4	Correction Factor for CAT Analysis Results	155

<i>Contents</i>		vii
5	Coronal Hole Size Dependence of Solar Wind Velocity	158
6	Slow Solar Wind from a Small Coronal Hole	159
7	N-S Asymmetry of High-Latitude Fast Solar Wind	163
8	Velocity Gradient in High-Speed Region	165
9	Bimodal Structure of Solar Wind Velocity	167
10	Summary of Solar Cycle Dependence	170
11	Solar Wind Velocity and Physical Condition in Corona	170
	11.1 Data	171
	11.2 Cross-Correlation Analysis	172
12	Conclusion	174
7		
	The Dynamically Coupled Heliosphere	179
	<i>Nathan Schwadron</i>	
1	Introduction	179
2	Inner Source of Pickup Ions	181
3	Distant Cometary Tails	183
4	Outer Source of Pickup Ions and Anomalous Cosmic Rays	186
5	Ubiquitous Statistical Acceleration	187
6	Magnetic Footpoint Motions Through Speed Transitions and Resulting Particle Acceleration	189
7	FALTS	192
8	Summary	195
8		
	A Global Picture of CMEs in the Inner Heliosphere	201
	<i>N. Gopalswamy</i>	
1	Introduction	201
2	Solar Source of CMEs	202
3	CME Morphology	203
4	Physical Properties	206
5	Statistical Properties	207
	5.1 CME Speed	208
	5.2 CME Acceleration	208
	5.3 CME Width	211
	5.4 CME Latitude	211
	5.5 CME Occurrence Rate	212
	5.6 CME Mass and Energy	213
	5.7 Halo CMEs	215
6	Associated Activities	218
	6.1 Flares and CMEs	219
	6.2 Prominence Eruptions	220
	6.3 Are There Two types of CMEs?	221
	6.4 X-ray Ejecta	221
	6.5 CMEs and Radio Bursts	222
	6.6 CME Interaction and Radio Emission	225
7	CMEs and Solar Energetic Particles	226
8	CMEs in the Heliosphere	229
	8.1 High Latitude CMEs	231
9	CMEs and Solar Polarity Reversal	232
10	CMEs and Cosmic Ray Modulation	233
11	Some Outstanding Questions	236
	11.1 CME Initiation	236
	11.2 How do CMEs Evolve?	237

12	Summary	240
9	MHD Turbulence in the Heliosphere: Evolution and Intermittency	253
	<i>Bruno Bavassano, Roberto Bruno and Vincenzo Carbone</i>	
1	Introduction	254
2	MHD Turbulence Evolution	255
	2.1 Ecliptic Turbulence	256
	2.2 Polar Turbulence	258
	2.3 Conclusions on Turbulence Evolution	263
3	Intermittency	264
	3.1 Probability Distribution Functions of Fluctuations and Self-similarity	269
	3.2 Radial Evolution of Intermittency	271
	3.3 Identifying Intermittent Events	273
	3.4 Conclusions on Intermittency	277
10	Waves and Turbulence in the Solar Corona	283
	<i>Eckart Marsch</i>	
1	Introduction	284
2	Coronal Magnetic Field Structures	284
3	Magnetic Network Activity and Coronal Heating	287
4	Waves and Flows in Loops and Funnels	290
5	Magnetohydrodynamic Waves and Flux Tube Oscillations	293
	5.1 Observation and Theory	293
	5.2 Oscillations of Thin Flux Tubes	295
	5.3 Wave Amplitudes Versus Height from Numerical Models	298
	5.4 A Standing Slow Magnetoacoustic Wave	299
6	Plasma Waves and Heating of Particles	301
7	Generation, Transfer and Dissipation of Coronal Turbulence	303
	7.1 Generation of Magnetohydrodynamic Waves	303
	7.2 Wave Energy Transfer and Turbulent Cascade	304
	7.3 Wave Dissipation in the Kinetic Domain	307
	7.4 Origin and Generation of Coronal High-Frequency Waves	308
	7.5 Ion Velocity Distribution and Wave Absorption	310
8	Summary and Conclusion	313
11	The Influence of the Chromosphere-Corona Coupling on Solar Wind and Heliospheric Parameters	319
	<i>Øystein Lie-Svendsen</i>	
1	Introduction	320
2	Closed Coronal Loops	322
3	The Modelling Tools	325
4	The Electron-Proton Solar Wind	331
5	Helium in the Corona and Solar Wind	341
6	Summary	349
12	Elemental Abundances in the Solar Corona	353
	<i>John C. Raymond</i>	

<i>Contents</i>		ix
1	Introduction	353
2	Methods	355
	2.1 Coronal Observations	355
	2.2 Solar Wind Measurements	357
3	FIP Effect	357
	Flares	359
	Active regions	359
	Quiet Sun	360
	Coronal Holes	360
	Prominences	361
	Coronal Mass Ejections	361
	Average Coronal FIP Bias	361
	Solar Wind	362
4	Gravitational Settling	363
5	Comparison with Other Stars	366
6	Summary	367
13		
	The Magnetic Field from the Solar Interior to the Heliosphere	373
	<i>Sami K. Solanki</i>	
1	Introduction	373
2	Solar Interior	374
3	Solar Surface	375
4	Chromosphere and Corona	380
5	The Heliosphere	386
6	Conclusion	389
14		
	Magnetic Reconnection	397
	<i>E. R. Priest and D. I. Pontin</i>	
1	Introduction	397
2	Two-Dimensional Reconnection	399
	2.1 X-Collapse	399
	2.2 Sweet-Parker Reconnection	400
	2.3 Stagnation-Point Flow Model	401
	2.4 Petschek's Model	402
	2.5 More Recent Fast Mechanisms	403
3	Three-Dimensional Reconnection	405
	3.1 Structure of a Null Point	405
	3.2 Global Topology of Complex Fields	405
	3.3 3D Reconnection at a Null Point	407
4	Three-Dimensional Reconnection at an Isolated Non-Ideal Region	408
	4.1 Fundamental Properties of 3D Reconnection	409
	4.2 Analytical Solutions for 3D Reconnection	410
5	Heating the Solar Corona by Reconnection	412
	5.1 Converging Flux Model	413
	5.2 Binary Reconnection	413
	5.3 Separator Reconnection	414
	5.4 Braiding	414
	5.5 Coronal Tectonics	415
6	Reconnection in the Magnetosphere	416
	6.1 Dayside Reconnection	417
	6.2 Nightside Reconnection	418

x *THE SUN AND THE HELIOSPHERE AS AN INTEGRATED SYSTEM*

7 Conclusions

419

Chapter 14

MAGNETIC RECONNECTION

E. R. Priest
and D. I. Pontin

Department of Mathematics

University of St Andrews

St Andrews

KY16 9SS, UK.

Abstract Magnetic reconnection is a fundamental process in a cosmic plasma such as the solar corona, responsible for heating and for many dynamic phenomena. We here review briefly the basic theory of reconnection in two dimensions and then proceed to describe several features of the way it operates in three dimensions. These include a description of 3D null points, of 3D topology, and of spine, fan and separator reconnection. Also an account of new properties of 3D reconnection at an isolated diffusion region is given, including the fact that a unique field line velocity can no longer be defined and that field line connections change continuously while a field line is traversing the non-ideal region. A summary is given of the various ways in which the corona may be heated, including binary, separator and braiding reconnection, as well as heating by coronal tectonics. Finally, a summary is also given of reconnection processes in the Earth's magnetosphere.

1. Introduction

In most of the universe magnetic field lines are frozen into the plasma and are carried about with it. However, in tiny current sheets the field lines are able to slip through the plasma, break and re-join. This process of magnetic reconnection is a fundamental one that is responsible for many dynamic phenomena in the cosmos (for a review, see the book by Priest & Forbes, 2000). It can change the topology of the magnetic field, and converts inflowing magnetic energy into heat, bulk kinetic energy and fast particle energy.

At the boundary of the Magnetosphere reconnection mediates a transfer of magnetic flux between the solar wind and the Earth's magnetic field. It occurs in both a steady and impulsive way at the front of the Magnetopause (so-called "flux transfer events") and also in the geomagnetic tail (in so-called "geomagnetic substorms"). It is also likely to be a major contributor to solar coronal heating and is certainly the process at the core of a solar flare.

We shall here be discussing reconnection in a magnetohydrodynamic (or MHD) plasma which satisfies the following equations: the plasma velocity \mathbf{v} and magnetic field \mathbf{B} are essentially determined by an equation of motion

$$\rho \frac{d\mathbf{v}}{dt} = -\nabla p + \mathbf{j} \times \mathbf{B} \quad (14.1)$$

and the induction equation

$$\frac{\partial \mathbf{B}}{\partial t} = \nabla \times (\mathbf{v} \times \mathbf{B}) + \eta \nabla^2 \mathbf{B}, \quad (14.2)$$

where the current (\mathbf{j}) is given by Ampère's law

$$\mathbf{j} = \frac{\nabla \times \mathbf{B}}{\mu}, \quad (14.3)$$

the pressure (p) by the perfect gas law

$$p = R \rho T, \quad (14.4)$$

the density (ρ) by the equation of continuity

$$\frac{\partial \rho}{\partial t} + \nabla \cdot (\rho \mathbf{v}) = 0, \quad (14.5)$$

and finally the temperature (T) by an energy equation.

In the induction equation (14.2), the ratio of the second term to the third term is the magnetic Reynolds number

$$R_m = \frac{L_0 v_0}{\eta}, \quad (14.6)$$

in terms of the typical plasma velocity (v_0) and scale (L_0) for variations. In most of the universe R_m is extremely large (of order $10^6 - 10^{12}$ typically) and so the first term on the right of (14.2) dominates, which implies that the magnetic field is tied to the plasma and moves with it, hanging onto its energy. The exception is in current singularities where the electric current is extremely large and the gradients of the magnetic field are enormous. They tend to form as sheets, often, although not

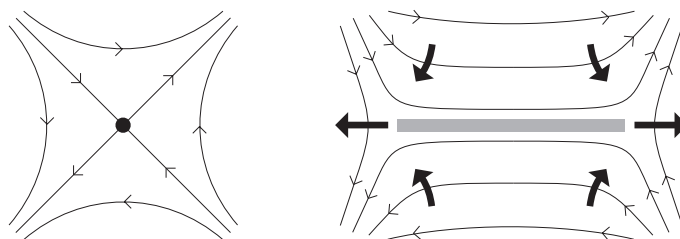


Figure 14.1. (a) The magnetic field lines near an X-type null point, where the magnetic field vanishes. (b) The collapse of this null point to form a current sheet.

only, at null points, where the magnetic field vanishes. It is in these singularities that the second term in the right of (14.2) becomes important and the magnetic field can diffuse through the plasma and reconnect.

In Section 2 we give a summary of reconnection in two dimensions, and then in Section 3 we describe some of the attempts to generalise these ideas to three dimensions. Section 4 gives a new analysis of how 3D reconnection occurs at an isolated diffusion region, highlighting just how different 3D reconnection is from its 2D counterpart. Section 5 summarises some of the ways in which reconnection could be heating the solar corona, including the latest idea of coronal tectonics. Finally, Section 6 describes reconnection processes occurring within the Earth's magnetosphere.

2. Two-Dimensional Reconnection

2.1 X-Collapse

Magnetic reconnection in two dimensions can occur in several ways. It can be driven by external motions, it can occur spontaneously due to the onset of an instability, or it can occur when an X-type null point collapses (Figure 14.1).

The linear field near a potential X-point can be written

$$\mathbf{B} = y \hat{\mathbf{x}} + x \hat{\mathbf{y}}, \quad (14.7)$$

where the current

$$j_z = \frac{\partial B_y}{\partial x} - \frac{\partial B_x}{\partial y} \quad (14.8)$$

vanishes and so this field is in equilibrium with itself. Now consider a perturbation of this field so that it becomes

$$\mathbf{B} = y \hat{\mathbf{x}} + \alpha^2 x \hat{\mathbf{y}}. \quad (14.9)$$

Whereas the field lines of (14.7) are rectangular hyperbolae $y^2 - x^2 = \text{const}$ with separatrices at right angles, those of (14.9) are hyperbolae

with separatrices $y = \pm\alpha x$, which are therefore closed up towards the y -axis if $\alpha > 1$. The resulting magnetic force

$$\mathbf{j} \times \mathbf{B} = \mu^{-1} (\alpha^2 - 1) (-\alpha^2 x \hat{\mathbf{x}} + y \hat{\mathbf{y}})$$

is in such a direction as to continue the perturbation and so, provided the field lines are not anchored and energy can propagate in towards the X-point, it tends to collapse, with α (and so the current)

$$j_z = \frac{\alpha^2 - 1}{\mu}$$

increasing indefinitely.

Linear solutions with magnetic diffusion included (Craig & McClymont, 1991) give collapse on a timescale of $t_A \log(R_m)$ together with a decaying oscillation, where t_A is the Alfvén travel time L_0/v_A , in terms of the Alfvén speed $v_A = B_0/(\mu\rho_0)^{1/2}$. Furthermore, non-linear self-similar solutions to the ideal equations of the form

$$\begin{aligned} B_x &= a(t)x + b(t)y, & B_y &= c(t)x + d(t)y, \\ v_x &= e(t)x + f(t)y, & v_y &= g(t)x + h(t)y, \\ p &= i(t)x^2 + j(t)xy + k(t)y^2 \end{aligned}$$

indicate that the collapse occurs in a finite time, although this analysis is only local (Imshennik & Syrovatsky; Klapper, 1998; Bulanov & Olshanetsky, 1984; Mellor et al., 2002).

2.2 Sweet-Parker Reconnection

In two-dimensions reconnection only takes place at an X-point, where the current can become very large and strong dissipation can allow the field lines to break and change their connectivity. In two dimensions the theory is well developed, with several mechanisms possible:

- 1 Slow Sweet-Parker reconnection (1958);
- 2 Fast Petschek reconnection (1964);
- 3 Many other fast regimes, depending on the boundary conditions, such as Almost-Uniform reconnection (Priest & Forbes, 1986) and Non-Uniform reconnection (Priest & Lee, 1990).

Sweet-Parker reconnection considers a simple current sheet of dimension l and L between two regions of uniform but oppositely directed

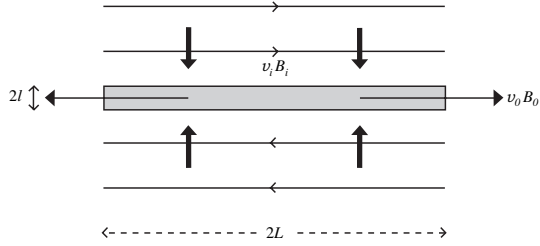


Figure 14.2 Sweet-Parker reconnection.

magnetic field (B_i) and flow (v_i) (Figure 14.2). It is just an order-of-magnitude model. Conservation of mass into and out of the sheet gives

$$L v_i = l v_0 \tag{14.10}$$

whereas for a steady state the balance between inwards advection and outwards diffusion gives

$$v_i = \frac{\eta}{l}. \tag{14.11}$$

Finally, the acceleration of plasma along the sheet by magnetic forces gives roughly

$$v_0 = v_{Ai}. \tag{14.12}$$

Eliminating l and v_0 between these three equations gives a dimensionless reconnection rate of

$$M_i = \frac{1}{R_{mi}^{1/2}}, \tag{14.13}$$

where $M_i = v_i/v_{Ai}$ is the Alfvén Mach number for the inflow and $R_{mi} = L v_{Ai}/\eta$ is the magnetic Reynolds number based on the sheet length (L) and the inflow Alfvén speed ($v_{Ai} = B_i / (\mu\rho)^{1/2}$).

In this mechanism the outflow magnetic field (B_0) is

$$B_0 = \frac{B_i}{R_m^{1/2}} \tag{14.14}$$

and so is much less than the inflow field (B_i) when $R_{mi} \gg 1$. Furthermore the inflow energy is mainly magnetic and half of it is transformed into kinetic energy while the other half is released as ohmic heating. In other words, the mechanism creates hot fast jets of plasma.

2.3 Stagnation-Point Flow Model

The stagnation-point flow model (Sonnerup & Priest, 1975) considers the effect of a stagnation-point flow

$$v_x = -U \frac{x}{a}, \quad v_y = U \frac{y}{a} \tag{14.15}$$

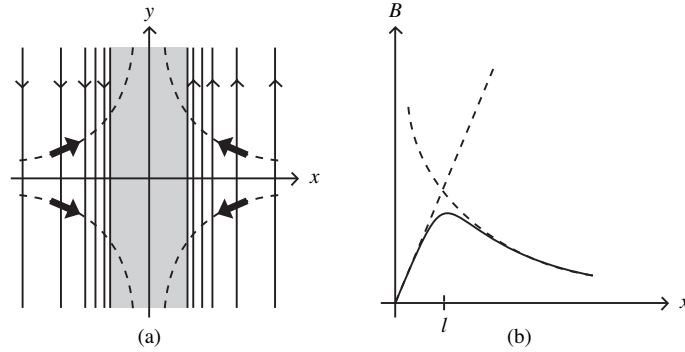


Figure 14.3. (a) Stagnation-point flow model, and (b) the variation with x of the magnetic field (B).

on a uni-directional magnetic field ($B(x)\hat{y}$), as shown in Figure 14.3(a). Ohm's law becomes

$$E - \frac{Ux}{a}B = \eta \frac{dB}{dx}, \quad (14.16)$$

where the electric field $E\hat{z}$ is uniform in space and constant in time. The solution for the magnetic field is

$$B(x) = \frac{2Ea}{v_0 l} e^{-x^2/l^2} \int_0^x e^{X^2/l^2} dX, \quad (14.17)$$

where $l^2 = 2\eta a/U$, as shown in Figure 14.3(b). It increases from 0 like Ex/η for small x and decreases like $Ea/(Ux)$ for $x \gg l$. At large distances the magnetic field is carried in towards the origin and is frozen to the plasma. At small distances it diffuses through the plasma in a current sheet of half-width l .

The advantage of the stagnation point flow model is that it is an exact solution of the MHD equations since it also satisfies the equation of motion. Furthermore, it has been generalised to produce so-called "reconnective annihilation" solutions in three dimensions, for both spine and fan geometries (Craig & Fabling, 1996). However, a limitation of the model is that the current sheet is purely one-dimensional and extends to infinity.

2.4 Petschek's Model

The main disadvantage of the Sweet-Parker model is that it is much too slow to explain reconnection in solar flares, and so Petschek (1964) proposed a much faster model in which the Sweet-Parker diffusion region is very much smaller. The diffusion region bifurcates to form two

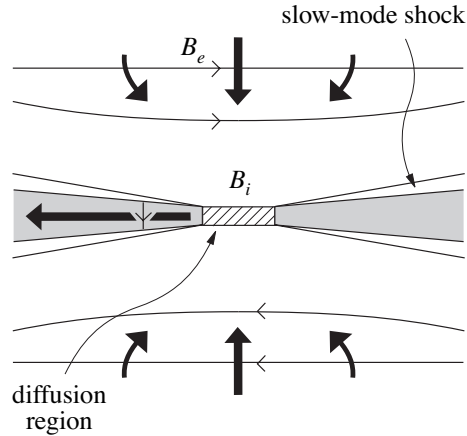


Figure 14.4 Petschek's model for fast reconnection

pairs of standing slow-mode shock waves at which most of the magnetic energy conversion takes place (Figure 14.4). Reconnection takes place at the rate at which it is driven at large distances. As the rate of reconnection increases, so the central diffusion region shrinks in size and the angle between each pair of shock waves increases. There is, however, a maximum allowable reconnection rate at which the mechanism chokes off. This has the form

$$M_{e \max} = \frac{\pi}{8 \log_e R_{me}}, \quad (14.18)$$

where $M_e = v_e/v_{Ae}$ is the ratio of the inflow speed to Alfvén speed (v_{Ae}) at large distances and $R_{me} = L_e v_{Ae}/\eta$ is the global magnetic Reynolds number based on the overall length-scale (L_e). Thus $M_{e \max}$ varies weakly with R_{me} and is typically 0.01 - 0.1 in magnitude.

2.5 More Recent Fast Mechanisms

The Almost-Uniform family of models (Priest & Forbes, 1986) include Petschek's model as a special case, but also it has a range of different regimes, depending on the boundary conditions at the inflow boundary (Figure 14.5). Regimes are classified by a parameter b , which determines the inclination of the streamline at the top right-hand corner of the region. Thus the regimes vary from strongly converging flows (14.5(a)) to strongly diverging flows - so-called "flux pile-up" reconnection (Figure 14.5(f)).

The Almost-Uniform family is characterised by an inflow region containing weakly curved magnetic field lines, but it is also possible for them to be strongly curved, as in the Non-Uniform family of models (Priest

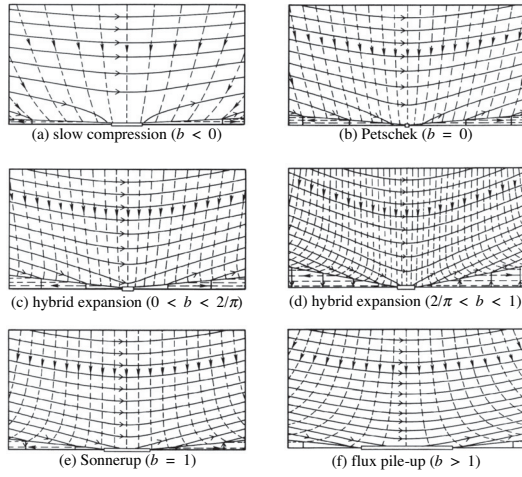


Figure 14.5 Almost uniform reconnection

& Lee, 1990). These exhibit jets of plasma expelled along the separatrices (field lines that pass through the X-point). Furthermore, this model agrees with the numerical experiments of Biskamp (1986) and of Yan et al. (1992,1993), provided the same boundary conditions are adopted (Strachan & Priest, 1994).

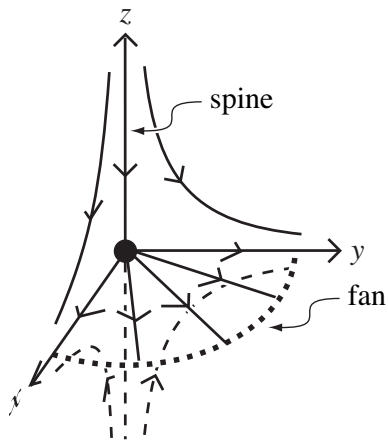


Figure 14.6 A 3D null point.

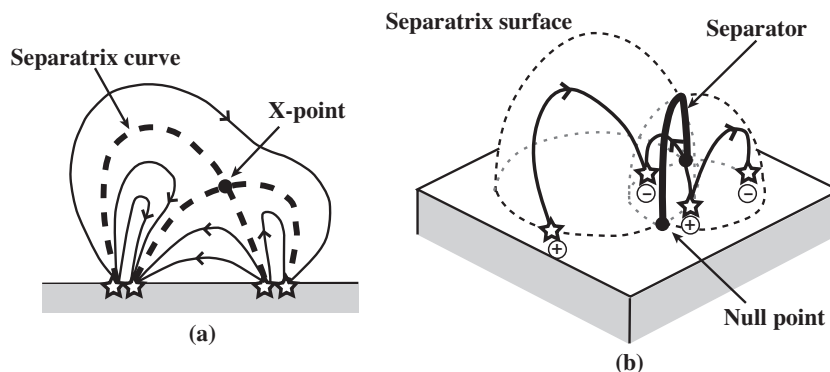


Figure 14.7. Topological structures (a) in 2D and (b) in 3D.

3. Three-Dimensional Reconnection

3.1 Structure of a Null Point

The simplest null point at the origin in three dimensions (Figure 14.6) has a magnetic field with components

$$(B_x, B_y, B_z) = (x, y, -2z), \quad (14.19)$$

with two families of field lines through the null: an isolated *spine* field line lies along the z -axis and approaches the null from both directions; a surface of *fan* field lines in the xy -plane recedes from the null.

Most generally, the linear field near a null may be written in the form (Parnell et al., 1996)

$$\begin{aligned} B_x &= x + \frac{1}{2}(q - J)y \\ B_y &= \frac{1}{2}(q + J)x + py \\ B_z &= jy - (p + 1)z \end{aligned}$$

in terms of parameters p , q , J and j , where J is the current along the spine and produces a twist in the fan, while j is the current in the fan and determines the angle between the spine and fan.

Just as in 2D, so in 3D a null can collapse to give a current growing along the spine or in the fan (Parnell, 1997).

3.2 Global Topology of Complex Fields

In two dimensions *separatrix curves* (which pass through X-type null points) separate the plane into topologically distinct regions, in the sense that field lines in a particular region all connect from one particular

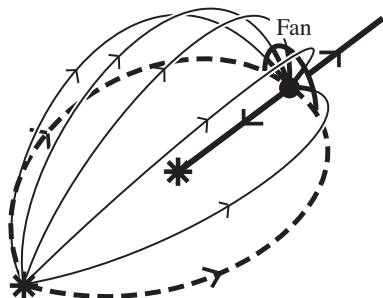


Figure 14.8 The skeleton of two unbalanced sources.

positive source to one particular negative source (Figure 14.7(a)). In three dimensions the topology of a model solar coronal field due to a series of flux sources lying in a plane is similar, but now the volume above the plane is divided into topologically distinct volumes by separatrix surfaces, which are usually the extensions of fan surfaces from 3D nulls (Figure 14.7(b)).

The way to reveal the structure of a highly complex field is to plot its *skeleton*, namely the set of null points, separatrix surfaces and spine field lines. For example, the skeleton of two unbalanced sources (Figure 14.8) consists of a null, its spine, and its fan, which arches over to form a dome enclosing the weaker source.

In contrast, when there are three magnetic sources, eight different topologies are possible, as categorised by Brown and Priest (1999). You can change from one topology to another by means of a *bifurcation*, either *local* (when nulls are created or destroyed) or *global* (when there is no change in the number of nulls). These include a local separator bifurcation (when a separator joining two nulls is created or destroyed), a global spine-fan bifurcation (when the spine of one null lies in the fan of the other at the moment of bifurcation) and a global separator bifurcation (when two fan surfaces touch at the moment of bifurcation to form a separator). Higher order behaviour due to the presence of four or more sources includes the presence of multiple separators (which can interact, merge or separate) and the appearance of coronal null points which can lift off the plane in a local double-separator bifurcation (Brown & Priest, 2001). If we model the photospheric field as a series of point sources, we find that the number of null points in the plane is roughly equal to the number (N_s) of sources, whereas the number of coronal nulls is about 5- 10% N_s (Longcope et al., 2003).

3.3 3D Reconnection at a Null Point

Priest and Titov (1996) discovered three different types of reconnection at a 3D null, namely *spine reconnection*, when the current concentrates along the spine, *fan reconnection* when it concentrates along the fan and *separator reconnection* when it focuses along the separator joining one null point to another.

Consider steady ideal flow of a magnetic field (14.19), satisfying

$$\mathbf{E} + \mathbf{v} \times \mathbf{B} = \mathbf{0} \quad (14.20)$$

and

$$\nabla \times \mathbf{E} = \mathbf{0}. \quad (14.21)$$

Equation (14.21) implies that $\mathbf{E} = \nabla F$ and so the scalar product of \mathbf{B} with Equation (14.20) gives

$$\mathbf{B} \cdot \nabla F = 0 \quad (14.22)$$

which determines the value of F everywhere in terms of values on the boundary by integrating along field lines. Furthermore, the vector product of \mathbf{B} with Equation (14.20) then determines the plasma velocity normal to the field lines as

$$\mathbf{v}_\perp = \frac{\mathbf{E} \times \mathbf{B}}{B^2}. \quad (14.23)$$

If we impose a flow on the side boundary continuous across the fan, then a singularity arises along the spine, which one can try to resolve by diffusion. If instead a continuous flow is imposed on the top and bottom across the spine, then a singularity arises at the fan.

A separator is a field line joining two 3D nulls and in the generic case it represents the intersection of the two fans of the nulls. In a section across the separator the field topology resembles that of a 2D X-point, and so, just as in 2D an X-point can collapse, so in 3D a separator can collapse to form a current sheet along the separator (Figure 14.9)- and, when the neighbouring field lines are carried into the separator sheet by a locally 2D stagnation point flow, then we find separator reconnection.

Galsgaard and Nordlund (1997) conducted an interesting experiment where their initial configuration contained eight 3D null points and they followed the effect of imposing a shear flow on two of the boundaries. They used a high-order finite-difference scheme on a 100^3 staggered grid with a Reynolds number of 100 and found that a current sheet formed along the separator (Figure 14.10) and produced separator reconnection.

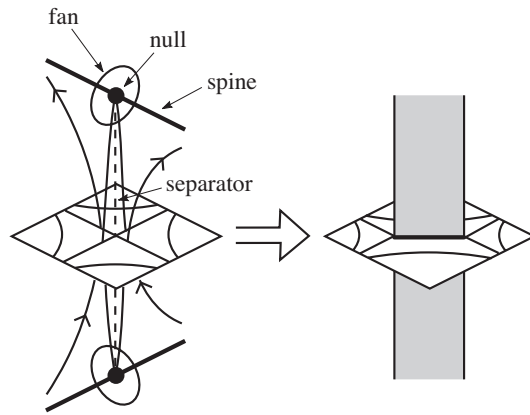


Figure 14.9 Collapse of a separator.

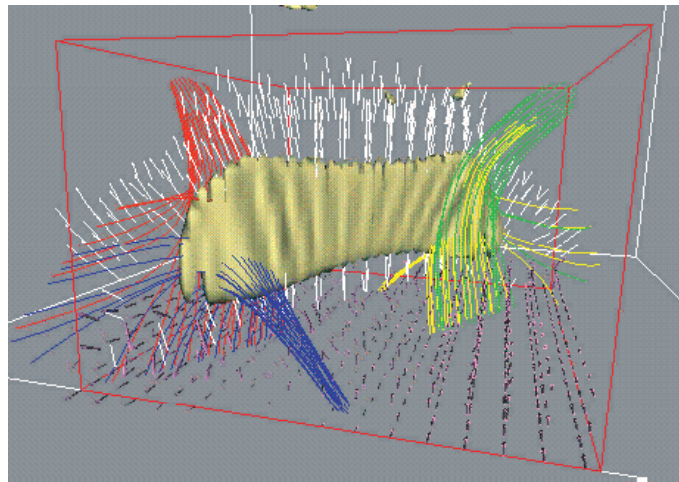


Figure 14.10. Numerical example of separator reconnection (?).

4. Three-Dimensional Reconnection at an Isolated Non-Ideal Region

Most astrophysical plasmas are effectively ideal, and non-ideal processes, which allow magnetic field lines to slip through the plasma, only become important on very small length scales. It is thus natural to consider reconnection processes which take place in isolated non-ideal regions. The resulting behaviour in 3D is fundamentally different from that in 2D.

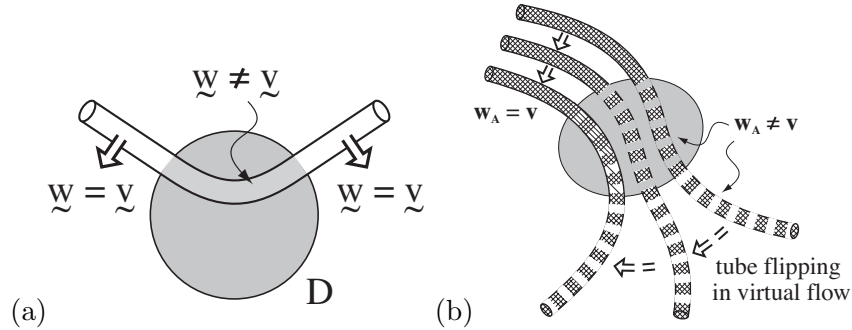


Figure 14.11. The behaviour of a flux tube which is partly within the non-ideal region (shaded) in (a) 2D and (b) 3D.

4.1 Fundamental Properties of 3D Reconnection

In 2D it is always possible to define a flux-conserving velocity (\mathbf{w}) which satisfies

$$\mathbf{E} + \mathbf{w} \times \mathbf{B} = \mathbf{0}, \quad (14.24)$$

and for reconnection to occur, \mathbf{w} must be singular at the X-point. Magnetic flux and field lines move everywhere at the velocity \mathbf{w} . By contrast, Priest et al. (2003a) have shown that in general in 3D a unique field line velocity does not exist, and consequently that a number of fundamental properties of 2D reconnection do not follow through when we consider reconnection in 3D. Several new properties of reconnection in 3D are listed below.

- 1 Since no unique field line velocity exists in 3D, field lines anchored in different regions of the ideal flow move in very different ways. In order to describe fully the motion of the magnetic flux in the volume, it is necessary to split the surface of the non-ideal region, D , into two parts, with magnetic flux entering D through one part and leaving it through the other. The field lines anchored in each of these regions move at completely separate velocities (though field lines which do not thread D move at the ideal plasma velocity everywhere as usual). Consequently, field lines which are followed through and beyond D appear to flip in a virtual flow (Figure 14.11).
- 2 Due to the non-existence of a unique field line velocity, magnetic field lines continually change their connections as they pass through D .

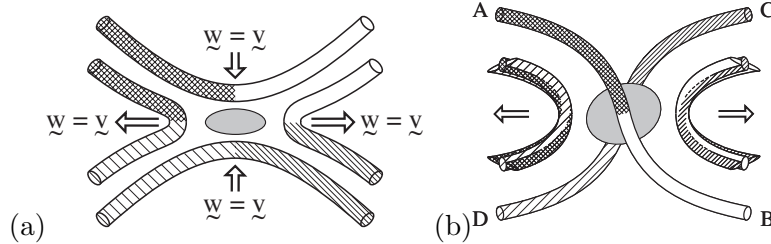


Figure 14.12. (a) Breaking and rejoining of flux tubes in 2D. (b) Breaking of two unique flux tubes in 3D showing partial rejoining, resulting in four distinct flux tubes after reconnection.

- 3 While the mapping between field line footpoints in 2D changes only at the X-point, where it is discontinuous, the mapping is generally continuous in 3D, the only exception being at separatrices of the field.
- 4 In 2D, magnetic field lines (and hence flux tubes) which undergo a reconnection process become rejoined in a simple one-to-one fashion. For every field line that is going to reconnect there is a corresponding field line with which it will rejoin perfectly. That is, their footpoints will become pair-wise oppositely connected after the field lines have undergone the reconnection process. The net effect is that before reconnection, we have two unique field lines and after reconnection we again have two unique, though differently connected, field lines (see Figure 14.12(a)).

The situation in 3D is very different. In general, for a given field line which is going to undergo reconnection, there is no corresponding counterpart field line with which its footpoints will become pair-wise oppositely connected after the reconnection process. The same is thus true in general for flux tubes (Figure 14.12(b)).

4.2 Analytical Solutions for 3D Reconnection

The study of reconnection is a highly complex one, which is as yet only in its very early stages. It is thus instructive to seek insight into the basic structure of the process by considering only a reduced set of the MHD equations. A number of analytical three-dimensional solutions, which we shall describe below, have been found. These solutions are kinematic, that is, they satisfy only the induction equation (14.2) as well as Maxwell's equations, but they do not satisfy the equation of motion (14.1). The state is assumed to be steady and a resistive non-ideal term

is considered. The equations solved are thus

$$\mathbf{E} + \mathbf{v} \times \mathbf{B} = \eta \mathbf{j}, \quad (14.25)$$

$$\nabla \times \mathbf{E} = \mathbf{0}, \quad (14.26)$$

$$\nabla \cdot \mathbf{B} = 0, \quad (14.27)$$

$$\nabla \times \mathbf{B} = \mu_0 \mathbf{j}, \quad (14.28)$$

where η is assumed to be localised in order to localise the effect of the non-ideal term on the right of (14.25).

In 3D, reconnection can occur either at null points or in their absence (Schindler et al., 1988). Hornig and Priest (2003) solved Equations (14.25)-(14.28) for the situation where there is no null point of the magnetic field. They imposed the steady magnetic field $\mathbf{B} = B_0(y, kx, b_0)$, a 2D X-point with uniform field in the third direction. The current is then given by $\mathbf{j} = ((k - 1)/\mu_0) \hat{\mathbf{z}}$. The imposed resistivity (η) is localised within a region D , centred on the origin. The resulting plasma flow is rotational, with oppositely directed rotation, around the z -axis, above and below D . The nature of the reconnection of magnetic flux is thus rotational as well, with field lines traced from footpoints anchored in the ideal region above D rotating in one sense, while those anchored below rotate in the opposite sense. Hence, in an arbitrarily short period of time, every field line which threads D changes its connection in this rotational fashion. The breakdown of the one-to-one correspondence of reconnecting field lines, and in general flux tubes, is also demonstrated.

Reconnection at a 3D null point with a localised diffusion region centred on the null has been considered by Pontin et al. (2004b) and Pontin et al. (2004a). The nature of the restructuring of magnetic flux is found to be profoundly different depending on the orientation of the electric current with respect to the null.

Pontin et al. (2004b) considered reconnection in the magnetic field $\mathbf{B} = B_0 \left(x - \frac{iy}{2}, y + \frac{jx}{2}, -2z \right)$, so that $\mathbf{j} = (B_0 j / \mu_0) \hat{\mathbf{z}}$ is parallel to the spine of the null. The ideal plasma flows, and thus the restructuring of the magnetic flux, are again found to be rotational. This rotation is once again centred on the axis along which the current is directed, the z -axis, and again has opposite sense above and below the null point. There is no flow across either the spine or fan, which lie along the z -axis and in the $z = 0$ plane respectively.

The case where the current is parallel to the fan plane is described by Pontin et al. (2004a). They consider the magnetic field $\mathbf{B} = B_0(x, y - jz, -2z)$, so that $\mathbf{j} = (B_0 j / \mu_0) \hat{\mathbf{x}}$. The fan of the null again lies in the $z =$

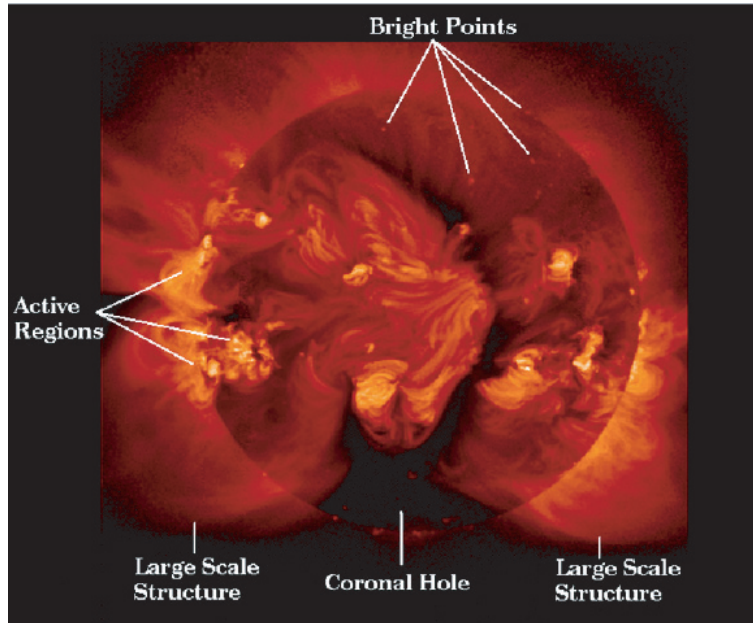


Figure 14.13. The solar corona from the Yohkoh satellite.

0 plane and the spine lies along $x = 0, y = jz/3$. This time the behaviour of the field lines is found to be much closer to that seen in the spine and fan reconnection of Priest and Titov (1996). The plasma flow is found to have a roughly stagnation point structure in planes of constant x , crossing both the spine and the fan. Field lines flip in constant succession around the spine line and through the fan plane. Solutions are also found where these two processes can be decoupled, so that the flow crosses only either the spine or fan, and so the field lines behave only either as in spine or fan reconnection. The existence of solutions with fan-crossing flows is particularly important in, for example, coronal fields on the Sun, since a transport of flux across the fan implies a change in the topology of the magnetic field.

5. Heating the Solar Corona by Reconnection

The solar corona at a temperature of a few million degrees consists of X-ray bright points, coronal loops and coronal holes. It is a magnetic world with myriads of magnetic interactions continually taking place (Figure 14.13). Recent space observations have shown examples of low-frequency waves being excited by solar flares (e.g. Nakariakov & Ofman, 2001), but these have too low an amplitude to be heating the corona.

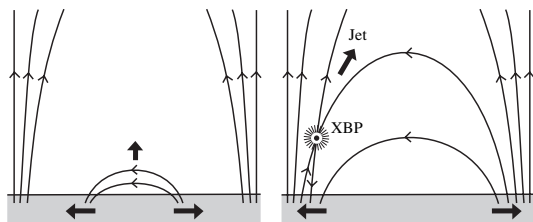


Figure 14.14 Converging flux model for X-ray bright points.

Also, there is a suggestion from broadening of UVCS lines in SOHO that high-frequency waves may be heating the outer corona. However, most of the evidence for heating the low corona is in favour of magnetic reconnection, which provides an elegant explanation for many diverse phenomena.

Yohkoh observations show that the hottest loops are cusps or interacting loops (Yoshida & Tsuneta, 1996). X-ray jets appear to be accelerated by reconnection (Shibata et al., 1992). Large-scale loops appear to have their upper coronal parts heated uniformly, which is consistent with turbulent reconnection (Priest et al., 1998). Furthermore, explosive events observed by SUMER on SOHO reveal that reconnection jets (Innes, Inhester, Axford, & Wilhelm, 1997) and nanoflares too may be caused by turbulent reconnection in myriads of current sheets.

5.1 Converging Flux Model

Reconnection is likely to be heating the corona in a variety of ways. First of all, X-ray bright points appear to be heated mainly by reconnection in cancelling magnetic flux (Parnell et al., 1994). The idea here is that new magnetic flux is continually emerging in supergranule cells as ephemeral regions, and the flux is swept to the edge of a cell, where it reconnects with the network flux and creates an X-ray bright point (Figure 14.14).

5.2 Binary Reconnection

There are many tiny discrete sources of magnetic flux on the solar surface and so it is natural to consider the “binary” interaction due to the relative motion of pairs of magnetic sources. Suppose they are unbalanced and connected - then the skeleton of the magnetic field is as shown in Figure 14.8. As the sources move, heat will be released in a process called *binary reconnection* (Priest et al., 2003b), which has several elements. First of all, the relative motion generates waves which propagate up and dissipate. Secondly, when the motions are slow, a non-linear force-free field is built up below the separatrix dome and then

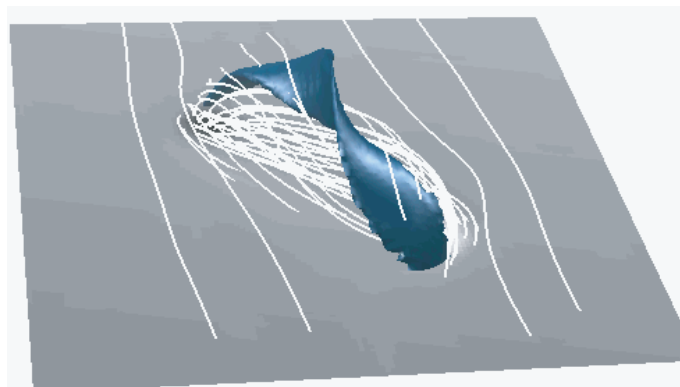


Figure 14.15. Separator reconnection (Parnell & Galsgaard, 2003).

dissipates by turbulent relaxation to a linear force-free state of lowest energy. Finally, reconnection occurs at the null and at the separatrix dome, both in a driven way and also spontaneously by tearing in the separatrix current sheet.

5.3 Separator Reconnection

The relative motion of two sources that are initially unconnected, although have an overlying field, has been considered by Parnell and Galsgaard (2003). They find that reconnection occurs along a twisted current sheet that forms along a separator. This produces a twisted flux tube joining the two sources, but the subsequent reconnection as the sources separate is rather weak. Various aspects of coronal heating by separator reconnection have also been considered by Longcope (1996, 1998).

5.4 Braiding

Parker (1979) proposed that braiding of the footpoints of coronal field lines can lead to the formation and subsequent dissipation of current sheets at the boundaries between neighbouring flux tubes. In his model he starts with a uniform field stretched between two planes which model the photosphere at two ends of a coronal loop. Also he imposes highly nonlinear complex braiding motions of the footpoints. The reality of the resulting formation of current concentrations has been demonstrated in a numerical experiment by Galsgaard and Nordlund (1996).

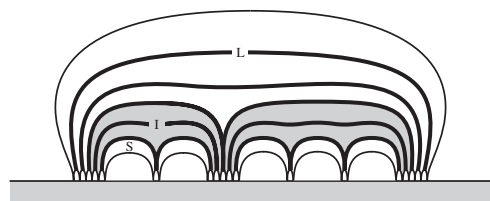


Figure 14.16 Coronal tectonics model.

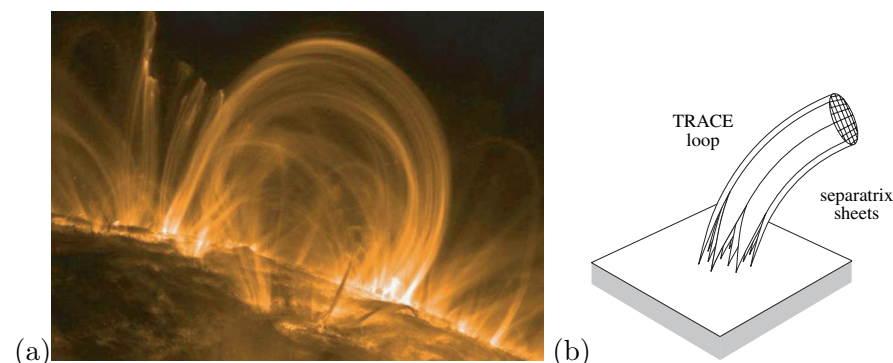


Figure 14.17. (a) TRACE coronal loops. (b) A web of separatrices within one loop.

5.5 Coronal Tectonics

In a new Coronal Tectonics Model for coronal heating, Priest, Heyvaerts and Title (2002) have attempted to model the effect of the *magnetic carpet* (Schrijver et al., 1998) on the corona. The magnetic sources in the photosphere are concentrated and continually move around so that the magnetic flux in the quiet Sun is processed every 14 hours (Hagenaar, 2001). Each observed coronal loop goes down through the surface in many discrete sources, so that the flux from each source is topologically distinct and separated by a network of separatrix surfaces that thread the corona. As the sources move so the coronal fluxes slip past one another and form myriads of separator and separatrix current sheets which heat impulsively by reconnection.

The fundamental flux units are tiny intense flux tubes of field $1200G$, diameter $100km$ and flux $3 \times 10^{17}Mx$. Thus a single X-ray bright point has 100 such sources, and each of the finest TRACE loops (Figure 14.17(a)) consists of 10 finer loops (Figure 14.17(b)), which reach the surface in many footpoints and within which there is a web of separatrices.

We have set up a model demonstrating how current sheets form between flux tubes and have estimated the heating. In addition, Mellor et al. (2004) have conducted a numerical experiment. By comparison with

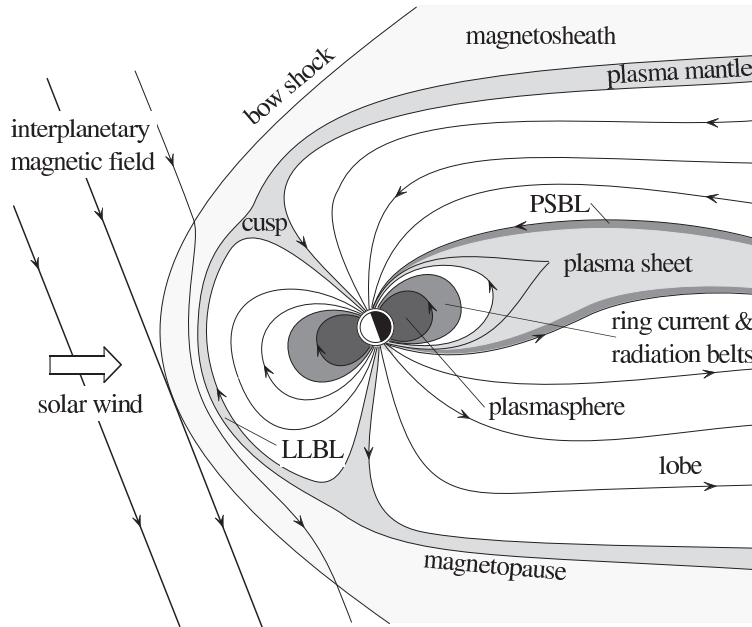


Figure 14.18. Schematic cross-section of the magnetosphere in the noon-midnight plane. LLBL and PSBL are acronyms for low-latitude boundary layer and plasma-sheet boundary layer respectively (after Parks, 1991).

Parker's braiding model, we have an array of coronal flux tubes going down to discrete sources in the photosphere in place of Parker's initial uniform field. Also our current sheets form immediately in response to simple generic motions of all kinds rather than requiring nonlinear braiding.

The results show that heating tends to be rather uniform along each separatrix implying that the elementary sub-telescopic tubes are heated uniformly. However, 90 - 95 % of the photospheric flux closes low down in the magnetic carpet, while the remaining 5 - 10 % forms large-scale connections. This suggests that the carpet should be heated more intensely than the large-scale corona. Also, unresolved observations of coronal loops would show enhanced heating near their feet in the carpet, with the upper parts of coronal loops being heated uniformly and less strongly.

6. Reconnection in the Magnetosphere

Magnetic reconnection is an important process not only on the Sun, but also closer to home in the Earth's own magnetosphere (see Figure

14.18). This is despite the fact that the plasma conditions are very different, being almost completely collisionless. Reconnection here too may occur in many different ways, which can be described in terms of an ‘open’ model of the magnetosphere, first proposed by Dungey (1961). It is termed as such because in the model a finite amount of magnetic flux connects the Earth to interplanetary space. In this model there are two neutral points on the dayside and nightside of the magnetopause, and the amount of reconnection which occurs depends strongly on the North-South orientation of the interplanetary magnetic field (IMF) carried by the solar wind. Reconnection can occur in the vicinity of both the dayside and nightside neutral points, as described below.

6.1 Dayside Reconnection

Dayside reconnection was for a long time less studied than its nightside counterpart, since it primarily leads to magnetic energy storage rather than release, and therefore has less obvious direct physical effects (Cowley, 1980). The reconnection is strong when the southward component of the IMF is large at the magnetopause, as this component is anti-parallel to the Earth’s magnetic field. Reconnection occurs here in a number of processes.

Firstly, magnetospheric erosion (Aubrey et al., 1970) is a signature of reconnection switching on at the dayside due to a southward turning of the IMF. The erosion happens because there is no outward flow within the magnetosphere to transport magnetic flux towards the reconnection site, and so this site moves earthwards as the reconnection consumes the flux on its earthward side.

Reconnection may occur a quasi-steady way at the magnetopause, since in the open model of the magnetosphere there is a non-zero normal component of the magnetic field there. Different schemes exist for how this may take place such as *component merging*, where reconnection takes place along the magnetopause separator connecting the two neutral points (Sonnerup et al., 1981; Soward, 1982) and *anti-parallel merging* where reconnection occurs only in regions where the magnetospheric and magnetosheath fields are close to anti-parallel (Crooker, 1979).

Also, reconnection occurs on the dayside in localised transient events known as flux transfer events (FTEs). These have been interpreted (Russell & Elphic) as isolated flux tubes interconnecting the IMF and magnetospheric field (see Figure 14.19(a)). Two further models for FTEs that have been proposed are those of Scholer et al. (1988) and Southwood et al. (1988), which produce FTEs by episodic 2D reconnection (Figure 14.19(b)), and that of Lee and Fu (1985), which assumes that an

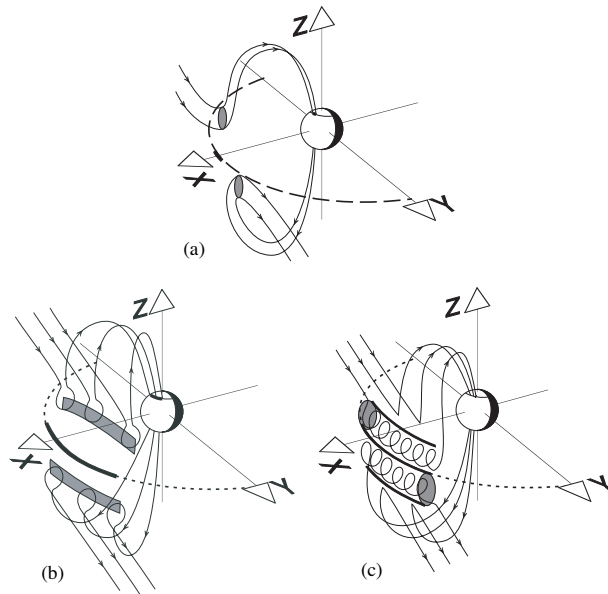


Figure 14.19 Three models for FTEs. The shaded areas indicate the cross-sections of the reconnected field lines at the surface of the magnetopause (after Lockwood, Cowley, & Sandholt, 1990).

FTE is a 2D magnetic island lying on the surface of the magnetopause (Figure 14.19(c)).

6.2 Nightside Reconnection

Reconnection on the nightside is very different. Here it occurs at a distant nightside neutral point, and converts magnetic energy into significant amounts of kinetic and thermal energy. Connected to this neutral point is an elongated current sheet which extends inwards towards the Earth. Importantly, observations have been made in the vicinity of the current sheet of slow-mode shocks (Feldman et al., 1984; Smith et al., 1984), with essentially the configuration predicted by Petschek, described earlier.

As well as occurring in the distant tail, nightside reconnection may also occur closer to the Earth in *magnetospheric substorms*. These are thought to take place when magnetic flux from dayside reconnection builds up in the tail, leading to a narrowing of the current sheet earthward of the nightside neutral point. This leads eventually to the creation of a further near-Earth neutral point. The result is that reconnection occurs, with a plasmoid being ejected down the tail, and earthward field lines relaxing back down to Earth, causing particles to be accelerated into bright aurorae. The phases of a substorm (see e.g. Hones, 1973) are shown in Figure 14.20.

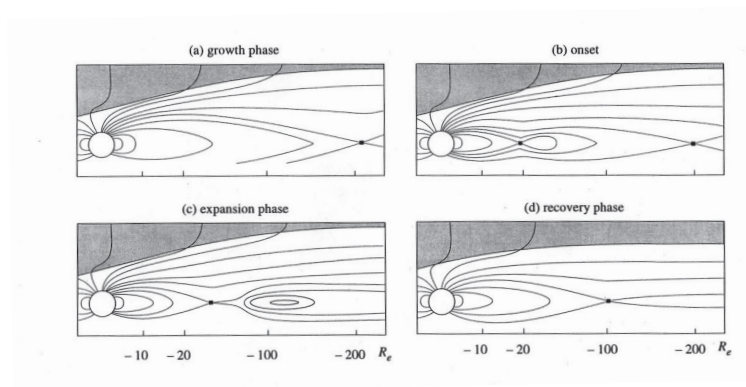


Figure 14.20. The phases of a magnetospheric substorm.

7. Conclusions

The theory of three-dimensional magnetic reconnection is in its infancy, but the indications are that reconnection can occur either in the absence of a null point or at a null point. In the latter case, spine reconnection, fan reconnection and separator reconnection are the main types that have been so far identified. Furthermore, 3D reconnection appears to be completely different from 2D reconnection in several aspects. Whereas field lines in 2D reconnect at a single point (the X-point), in 3D they continually change their connection as they pass through a non-ideal region. Furthermore, in 3D a unique field line velocity cannot be defined, since field lines anchored on one side of a non-ideal region behave differently to those anchored on the other side.

Several proposals have now been made for heating the Sun's corona by magnetic reconnection. X-ray bright points are thought to be due to reconnection driven by the motion of photospheric footpoints, mainly by converging motions. The high corona may possibly be heated by high-frequency waves, but the coronal loops could be heated by reconnection either due to binary reconnection or due to separator reconnection, or due to braiding. Another promising possibility is that coronal loops are driven by turbulent reconnection in myriads of current sheets by coronal tectonics. Furthermore, we have also seen that reconnection occurs in the Earth's magnetosphere, on both the dayside and the nightside.

In future, in order to understand the enigma of coronal heating there is an urgent need to: measure the temperature in coronal loops more accurately; understand fully the effect of the magnetic carpet; determine the effect of complex magnetic topology; unify our understanding of the zoo of coronal transients; test the viability of the Coronal Tectonics

Model; and, with the help of Solar B and Solar Dynamics Observatory, to understand properly the nature of the subtle link between the solar surface and corona.

Acknowledgments

We are grateful to the UK Particle Physics and Astronomy Research Council and the Carnegie Trust for financial support and to Terry Forbes, Gunnar Hornig, Jean Heyvearts, Dana Longcope and Slava Titov for fruitful discussions about the nature of 3D reconnection and coronal heating.

References

- Aubrey, M. P., C. T. Russell and M. G. Kivelson (1970), *J. Geophys. Res.*, 75, 7018-7031.
- Biskamp, D. (1986), *Phys. Fluids*, 29, 1520-1531.
- Brown, D. S., and E. R. Priest (1999), *Proc. R. Soc. Lond. A*, 466, 3931.
- Brown, D. S., and E. R. Priest (2001), *Astron. Astrophys.*, 367, 339-346.
- Bulanov, S. V., and M. A. Olshanetsky (1984), *Phys. Lett.*, 100, 35-38.
- Cowley, S. W. H. (1980), *Space Sci. Rev.*, 26, 217-275.
- Craig, I. J. D., & A. N. M. McClymont (1991), *Astrophys. J.*, 371, L41-L44. 5 pages = "L41-L44"
- Craig, I. J. D., & R. B. Fabling (1996), *Astrophys. J.*, 462, 969-976. 5 volume = "462",
- Crooker, J. U. (1979), *J. Geophys. Res.*, 84, 951-959.
- Dungey, J. W. (1961), *Phys. Rev. Lett.*, 6, 47-48.
- Feldman, W. C., S. J. Schwartz, S. J. Bame, D. N. Baker, J. Birn, J. T. Gosling, E. W. Hones, Jr., D. J. McComas, J. A. Slavin, E. J. Smith, & R. D. Zwickl (1984), *Geophys. Res. Lett.*, 11, 599-602.
- Galsgaard, K., & A. Nordlund (1996), *J. Geophys. Res.*, 101, 13445-13460.
- Galsgaard, K., & A. Nordlune (1997), *J. Geophys. Res.*, 102, 231-248.
- Hagenaar, H. J. (2001), *Astrophys. J.*, 555, 448-461.
- Hones, E. W., Jr. (1973), *Radio Sci.*, 8, 979-990.
- Hornig, G., & E. R. Priest (2003), *Physics of Plasmas*, 10(7), 2712-2721.
- Imshennik, V. S., & S. I. Syrovatsky (1967), *Sov. Phys. JETP*, 25, 656-664.
- Innes, D. E., B. Inhester, W. I. Axford, & K. Wilhelm (1997), *Nature*, 386, 811-813.
- Klapper, I. (1998), *Phys. Plasma*, 5, 910-914.
- Lee, L. C., & Z. F. Fu (1985), *Geophys. Res. Lett.*, 12, 105-108.

- Lockwood, M., S. W. H. Cowley, & P. E. Sandholt (1990), *EOS, Trans. Amer. Geophys. Union*, 71, 719-720.
- Longcope, D. W. (1996), *Solar Phys.*, 169, 91-121.
- Longcope, D. W. (1998), *Astrophys. J.*, 507, 433-442.
- Longcope, D. W., D. S. Brown, & E. R. Priest (2003), *Phys. Plasmas*, 10, 3321-3334.
- Mellor, C., V. S. Titov, & E. R. Priest (2002), *J. Plasma Phys.*, 68, 221-235.
- Mellor, C., C. Gerrard, K. Galsgaard, A. W. Wood, & E. R. Priest (2004), submitted for publication.
- Moffat, H. K. (1978), "Magnetic Field Generation in Electrically Conducting Fluids", Cambridge Univ. Press: Cambridge, UK.
- Nakariakov, V. M., & L. Ofman (2001), *Astron. Astrophys.*, 372, L53-L56.
- Parker, E. N. (1979), "Cosmical Magnetic Fields", Clarendon Press: Oxford.
- Parnell, C. E., E. R. Priest, & L. Golub (1994), *Solar Phys.*, 151, 57-74.
- Parnell, C. E., J. M. Smith, T. Neukirch, & E. R. Priest (1996), *Phys. Plasma*, 3(3), 759-770.
- Parnell, C. E., T. Neukirch, J. M. Smith, & E. R. Priest (1997), *Geophys. Astrophys. Fluid Dynamics*, 84, 245-271.
- Parnell, C. E., & K. Galsgaard (2003), submitted for publication.
- Parks, G. K. (1991), "Physics of Space Plasma", Addison-Wesley: Reading, Massachusetts, USA.
- Petschek, H. E. (1964), in "Magnetic Field Annihilation" (W. N. Hess, ed.), 425-439, NASA SP-50, Washington, D.C., USA.
- Pontin, D. I., G. Hornig, & E. R. Priest (2004), submitted for publication.
- Pontin, D. I., G. Hornig, & E. R. Priest (2004), submitted for publication.
- Priest, E. R., & T. G. Forbes (1986), *J. Geophys. Res.*, 91, 5579-5588.
- Priest, E. R., & L. C. Lee (1990), *J. Plasma Phys.*, 44, 337-360.
- Priest, E. R., & V. S. Titov (1996), *Phil. Trans. R. Soc. Lond. A*, 354, 2951-2992.
- Priest, E. R., C. R. Foley, J. Heyvaerts, T. D. Arber, J. L. Culhane, & L. W. Acton (1998), *Nature*, 393, 545-547.
- Priest, E. R., & T. G. Forbes (2000), "Magnetic Reconnection: MHD Theory and Applications", Cambridge Univ. Press: Cambridge, UK.
- Priest, E. R., J. F. Heyvaerts, & A. M. Title (2002), *Astrophys. J.*, 576, 533-551.
- Priest, E. R., G. Hornig, & D. I. Pontin (2003), *J. Geophys. Res.*, 108(A7), SSH6-1.

- Priest, E. R., D. W. Longcope, & V. S. Titov (2003), *Astrophys. J.*, 598, 667-677.
- Russell, C. T., & R. C. Elphic (1978), *Space Sci. Rev.*, 22, 681-715.
- Schindler, K., M. Hesse, & J. Birn (1988), *J. Geophys. Res.*, 93(A6), 5547-5557.
- Scholer, M. (1988), *Geophys. Res. Lett.*, 15, 748-751.
- Schrijver, C. J., A. M. Title, K. L. Harvey, N. R. Sheeley, Y. -M. Wang, G. H. J. van den Oord, R. A. Shine, T. D. Tarbell, & N. E. Hurlburt (1998), *Nature*, 394, 152-154.
- Shibata, K., V. Ishido, L. W. Acton, K. T. Strong, T. Hirayama, Y. Uchida, A. H. McAllister, R. Matsumoto, S. Tsuneta, T. Shimizu, H. Hara, T. Sakurai, K. Ichimoto, V. Nishino, & Y. Ogawara (1992), *Publ. Astron. Soc. Japan*, 44, L173-L179.
- Smith, E. J., J. A. Slavin, B. T. Tsurutani, W. C. Feldman, & S. J. Bame (1984), *Geophys. Res. Lett.*, 217, 644-656.
- Sonnerup, B. U. Ö., & E. R. Priest (1975), *J. Plasma Phys.*, 14, 283-294.
- Sonnerup, B. U. Ö., G. Paschmann, I. Papamastorakis, N. Sckopke, G. Haerendel, S. J. Bame, J. R. Asbridge, J. T. Gosling, & C. T. Russell (1981), *J. Geophys. Res.*, 86, 10049-10067.
- Southwood, D. J., C. J. Farrugia, & M. A. Saunders (1988), *Planet. Space Sci.*, 36, 503-508.
- Soward, A. M. (1982), *J. Plasma Phys.*, 28, 415-443.
- Strachan, N. R., & E. R. Priest (1994), *Geophys. Astrophys. Fluid Dynamics*, 74, 245-274.
- Sweet, P. A. (1958), in "Electromagnetic Phenomena in Cosmical Plasma", 123-134, Cambridge Univ. Press: London, UK.
- Yan, M., L. C. Lee, & E. R. Priest (1992), *J. Geophys. Res.*, 97, 8277-8293.
- Yan, M., L. C. Lee, & E. R. Priest (1993), *J. Geophys. Res.*, 98, 7593-7602.
- Yoshida, T., & S. Tsuneta (1996), *Astrophys. J.*, 459, 342-346.